Study on dynamic mechanical response of a polymer bonded explosive under high strain rates

XUANMING CAI, WEI ZHANG*, DACHENG LI, WENBO XIE
Hypervelocity Impact Research Center, Harbin Institute of Technology, Harbin 150080, China

Dynamic compressive stress-strain curves of a polymer bonded explosive (PBX) at high strain rates (from 403s^{-1} to 2207 s^{-1}) have been determined with a modified split Hopkinson pressure bar (SHPB). Pulse shaping was used to ensure that the PBX specimen deforms at a nearly constant strain rate under dynamically equilibrated stress. A nearly constant strain rate under dynamically equilibrated stress was provided based on the pulse shaping. The laser displacement meter was used to monitor the axial strain of the specimen in the experiments. The validity of the experiments was monitored by the polyvinylidene fluoride (PVDF) force sensors for dynamic stress equilibrium, and by a high-speed camera for specimen deformation. All results indicate that the material is sensitive to strain rate and the strain-rate sensitivity depends on the value of strain, and the compressive strength improves with the increase of RDX content.

(Received May 13, 2014; accepted March 19, 2015)

Keywords: PBX, Mechanical response, SHPB

1. Introduction

Polymer bonded explosives materials have an extensive application in the conventional warhead and rocket propellant [1-2]. With the rapid development of modern high-performance weapon system, improving the safety performance of PBX becomes increasingly urgent. In the process of high-speed penetration, the dynamic mechanical response of PBX directly impacts the safety performance of weapon equipment. Therefore, it is of great significance to study the dynamic mechanical response of PBX.

Zhou Zhong-bin et al. [3-5] carried out some researches on the dynamic deformation and microstructures of PBX substitute material. Liang Zeng-you et al. [6] conducted the shock tests to study the damage of PBX materials. Over the past decade, much progress on traditional energetic materials has been achieved, especially in mechanical properties [7-11], damage evolution [12], and high rate deformation [13-15]. In most available researches, the PBX materials are brittle. However, the PBX materials in this paper are viscoelastic, and it is a new phlegmatic high energetic material. And the dynamic mechanical properties of this material under high strain rates have been less known yet. In this paper, the dynamic compressive behavior of the PBX material is explored by a modified split Hopkinson press bar setup.

2 Experiments

2.1 Experimental materials and setup

Two kinds of PBX specimens (Φ16mm×4mm), PBX1 and PBX2, are fabricated by a pouring process. Forty percent of PBX1 is made of RDX, and the others is the mixtures of aluminum powder and polymer. And sixty percent of PBX2 is made of RDX, the others is the same mixtures with PBX1. They both have some similar characteristic with rubber.

A modified SHPB setup for low-impedance material testing is employed to conduct the dynamic compressive experiments on the PBX materials, as shown in Fig. 1. Considering the material impedance matching, the striker bar (Φ20mm×150mm), the incident bar (Φ20mm×1500mm) and the transmitted bar (Φ20mm×1500mm) are all made of LC4 aluminum. The specimen strains measured by strain gauges are stored by CD-1D high dynamic strain indicator. The axial strains of specimens are measured by laser displacement meter, and the stress states on both ends of the specimen are monitored by PVDF force sensors [16]. The deformation and failure process of the PBX materials are recorded by the high speed camera.

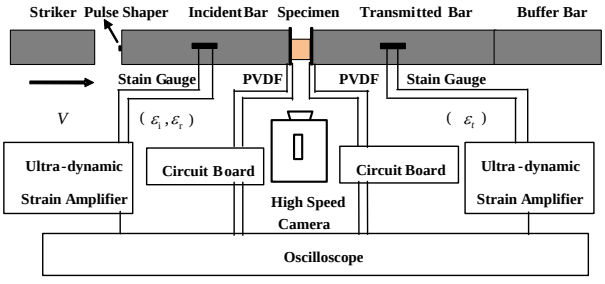

Fig. 1. Experimental setup.

2.2 Experimental principle

A striker bar impacting the incident bar of the same cross sectional area and modulus generates an elastic stress pulse. The elastic stress pulse propagates through the incident bar and passes through the specimen while deforming it. The impact velocity of the striker bar is twice as large as the particle velocity imposed on the incident bar [8]. When reaching the interface between the specimen and the incident bar, the part of the elastic stress pulse are reflected back, and the others are transmitted from the specimen and pass through the transmitted bar. Strain gages mounted on both the middle position of the incident and transmit bars are used to acquire the incident pulse, the reflected pulse and the transmitted pulse. Based on the assumption of one-dimensional wave propagation, it is meaningful to analyze the strain signals from the strain gages. The strain-rate $\dot{\varepsilon}(t)$, strain $\varepsilon(t)$ and stress $\sigma(t)$ of the specimen can be expressed as [17]

$$\dot{\varepsilon}(t) = -\frac{2C_0}{L_s}\varepsilon_R(t) \tag{1}$$

$$\varepsilon(t) = -\frac{2C_0}{L_s}\int_0^t \varepsilon_R(t)\mathrm{d}t \tag{2}$$

$$\sigma(t) = \frac{E_b A_b}{A_s}\varepsilon_T(t) \tag{3}$$

Where C_0 is the longitudinal wave velocity in the bar, L_s is the original length of the specimen, and ε_R and ε_T are the strain of the reflected and transmitted pulse, respectively. ε_I is the incident pulse. A_b and A_s are the cross sectional areas of the Hopkinson bars and the specimen, respectively. Based on the assumption of the dynamic stress equilibrium, it can be expressed as:

$$\varepsilon_I + \varepsilon_R = \varepsilon_T \tag{4}$$

2.3 Calibration of laser displacement meter

The laser displacement meter mainly includes laser, lens and receiver. And the working principle is that the displacement by blocking the light is obtained through monitoring the light-changed value of the laser. For static calibration, a set of high precision feelers is used to partly block the laser. The blocking length of the feelers ranges from 0 to 10mm with a step of 0.05mm. A certain amount of voltage ΔU is outputted through the photoelectric converter under a light-passing length Δd, as defined in Eq. 5.

$$\Delta U = K\Delta d \tag{5}$$

where k is the calibration parameter of the laser displacement meter. As shown in Fig. 2, it displays a good linearity, which indicates the high uniformity of the laser.

To verify the dynamic response frequency of the laser displacement meter system, the dynamic calibration is completed by a single Hopkinson bar under dynamic loading. The striker bar is used to impact one end of the incident bar, and the laser displacement meter system is used to monitor the motion of the other end. When the impact compressive wave arrives at the free end of the incident bar, it would be reflected as a tensile wave and then the free end of the incident bar begins to move. The incident and reflected waves are measured by the strain gauges glued on the middle of the incident bar. The displacement-moved of the free end of the incident bar can be defined as [18]

$$\Delta d = \int_0^t (\varepsilon_i + \varepsilon_r) C_0 d\tau \tag{6}$$

where t is the time of a shock compressive pulse, C_0 is the compressive wave velocity in the incident bar. Based on Eq. 5, the displacement of the free end of the incident bar can be measured with the output of the laser displacement meter system. The above displacement is compared with the value obtained by the strain gauges. As shown in Fig. 3, an excellent agreement suggests that the laser displacement meter system has enough dynamic response for measuring in SHPB. Chen et al. had completed the dynamic calibration with the above method [1], but the laser displacement meter in this paper is more advanced. Its dynamic response frequency 3.5MHz completely meets the requirements of SHPB dynamic loading. More importantly, its use is more convenient.

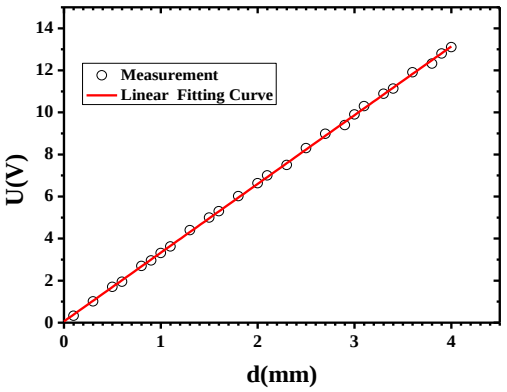

Fig. 2. Static calibration.

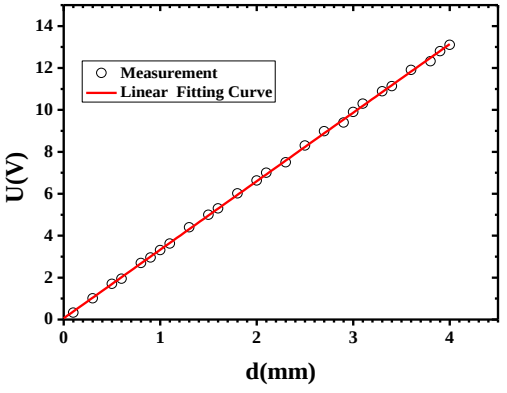

Fig. 3. Dynamic calibration.

3. Experiment results

To ensure the dynamic stress equilibrium and homogeneous deformation at a constant strain rate, a proper pulse shaper-rubber (Φ10mm×2mm) was applied to change the incident pulse, and the original signals under the strain rate of 860/s are shown in Fig. 4. The stress state on both ends of the specimen monitored by the PVDF force sensors, as shown in Fig. 5, also shows a great agreement. With the dynamic stress equilibrium, it ensures the experimental feasibility.

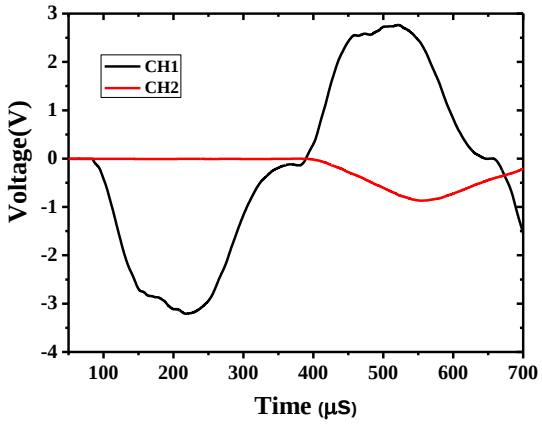

Fig. 4. The original voltage signals.

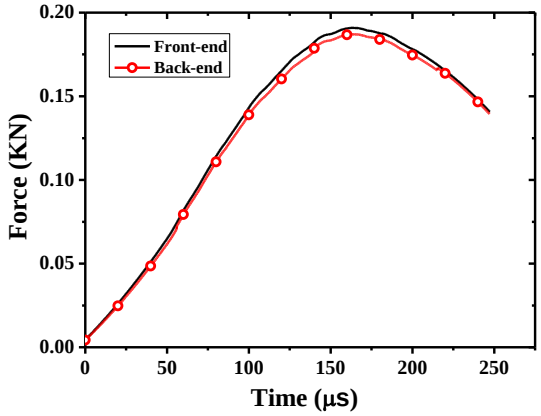

Fig. 5. Forces on the both ends of the specimen.

In the case of compression experiments

$$\frac{l}{l_0} = 1 - \varepsilon_E \tag{7}$$

$$\varepsilon_T = \ln(1+\varepsilon_E) \tag{8}$$

$$\sigma_T = \sigma_E(1+\varepsilon_E) \tag{9}$$

where l_0 and l are the original specimen thickness and the current specimen thickness, respectively. ε_E and ε_T are respectively the engineering strain of the specimen and the true strain of the specimen. σ_E and σ_T are the engineering stress of the specimen and the true stress of the specimen, respectively.

To improve observation of the deformation process of the specimen as indicated by the high-speed camera, scattered spots were sprayed on the surface of the specimen. Homogeneous deformation of the specimen is revealed, as shown in Fig. 6. The engineering strain value obtained from the laser displacement meter agree well with the one calculated from the signal value of the strain gauges in the incident bar and the transmitted bar, shown as in Fig. 7, and it shows that the laser displacement meter can be applied to the dynamic tests in the Hopkinson bar.

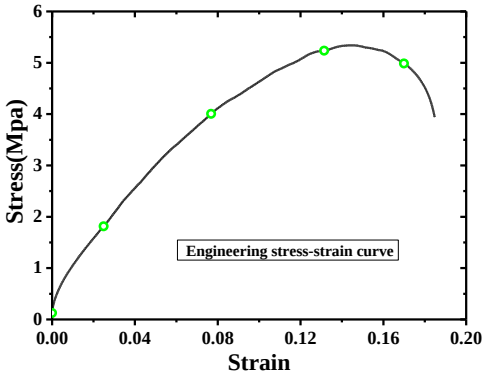

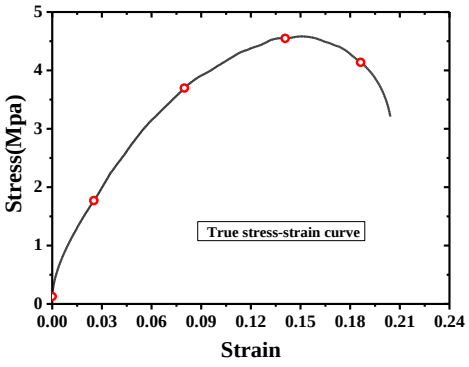

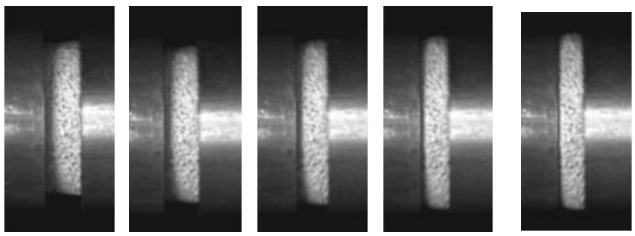

$0(t=0\mu s)$ $1(t=50\mu s)$ $2(t=100\mu s)$ $3(t=150\mu s)$ $4(t=200\mu s)$

Fig. 6. High-speed deformation of the PBX2 under the strain rate of 860/s.

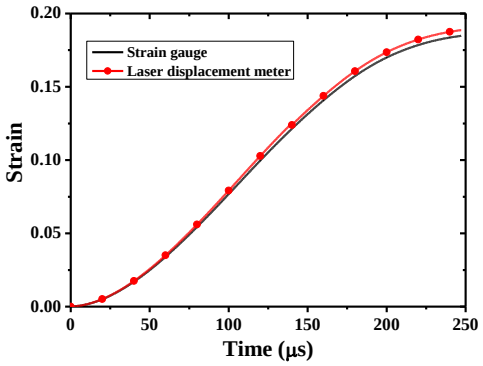

Fig. 7. Strain measured by the laser and strain gauges.

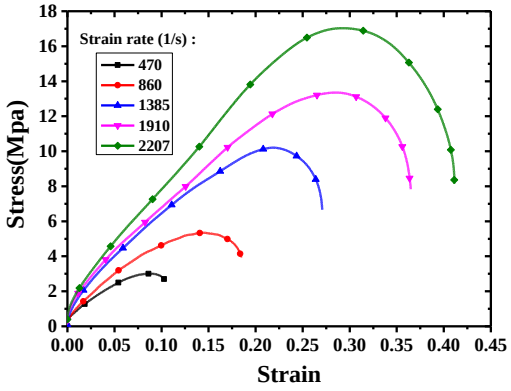

Fig. 8. Stress-strain curves of PBX1.

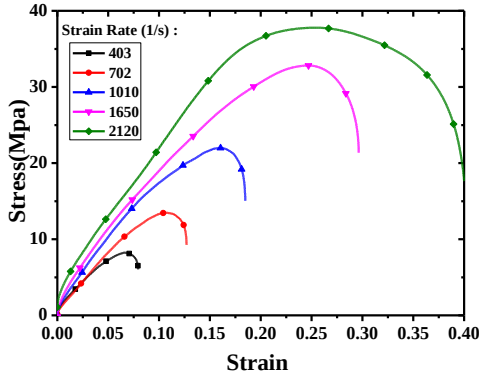

Fig. 9. Stress-strain curves of PBX2.

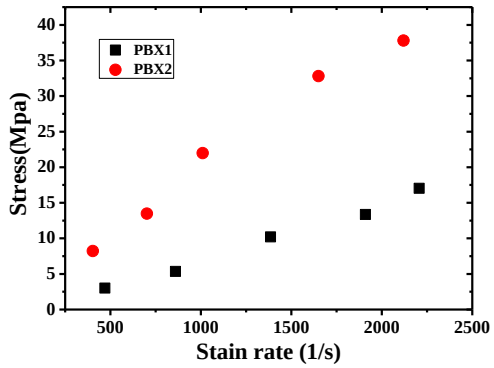

Fig. 10. The compressive strength VS strain rates.

The dynamic stress-strain curves of PBX1 under high strain rates (from $470s^{-1}$ to $2207s^{-1}$) indicate that the compressive strength improves with the increase of the strain rate, as shown in Fig. 8. The stress-strain curves of PBX2 have the same characteristic with PBX1, as shown in Fig. 9, but the compressive strength of PBX2 are greater than that of PBX1 in the similar strain rates (shown in Fig. 10). The results suggest that the PBX material is sensitive to strain rates.

4. Conclusions

The dynamic compressive behavior of polymer bonded explosive materials at high strain rates (from $403s^{-1}$ to $2207s^{-1}$) is determined with a modified SHPB for low-impedance material test. Pulse shaping is used to ensure that the PBX specimen deforms at a nearly constant strain rate under dynamically equilibrated stress. The PVDF force sensors are used to record the dynamic stress equilibrium processes on the both ends of the PBX substitute specimens. The laser displacement meter is used to monitor the axial strain of the specimen in the experiments. A high-speed camera was used to monitor the uniform deformation of the PBX specimens during SHPB experiments. These measures ensured that valid data were obtained during the SHPB experiments.

The experimental results show that the PBX material is sensitive to strain rates, and the strain-rate sensitivity depends on the value of strain. Its compressive strength improves with the increase of RDX content. The laser displacement meter can be applied to the SHPB setup system.

References

[1] R. Chen, Changsha: National University of Defense Technology, 19-36 (2010). (in china)
[2] H. Fu, J. L. Li, D. W. Tan, Chinese Journal Of High Pressure Physics, **26**(2), 148 (2012).
[3] Z. B. Zhou, P. W. Chen, F. L. Huang, Acta Armamentarii, **31**(1), 288 (2010).
[4] P. Zhang, F. Zhao, S. L. Bai, Chinese Journal of High Pressure Physics, **21**(1), 20 (2007).
[5] S. G. Grantham, C. R. Siviour, W. G. Proud, et al. Measurement Science and Technology, **15**(9), 1867 (2004).
[6] Z. Y. Liang, F. L. Huang, Zh. P. Duan, et al. Journal of Projectiles, Rockets, Missiles and Guidance, **28**(1), 132 (2008).
[7] D. Picart, J. L. Brigolle, Materials Science and Engineering **A527**, 7826 (2010).
[8] Chen Rong, Lu fanyun et al. Chinese Journal of Energetic Materials, **15**(5), 461 (2007).
[9] Han Xiaoping, Zhang Yuanchong, et al. Journal of Experimental Mechanics, **11**(3), 304 (1996).

[10] Wu Huimin, Lu Fanyun, Chinese Journal of High Pressure Physics, **19**(2), 140 (2005).
[11] Li Yinglei, Li Dahong, et al. Explosion and shock waves, **19**(4), 354 (1999).
[12] Xian Wang, Shaopeng Ma, Yingtao Zhao, Zhongbin Zhou, Pengwan Chen, Polymer Testing **30**, 861 (2011).
[13] Qi-Long Yan, Svatopluk Zeman, Ahmed Elbeih, Thermochimica Acta **537**, 1 (2012).
[14] J. E. Field, S. M. Walley, W. G. Proud, H. T. Goldrein, C. R. Siviour, International Journal of Impact Engineering **30**, 725 (2004).
[15] G. Goudrean, 1985: UCID-20358.
[16] X. J. Ren, H. L. Chen, Journal of Vibration and Shock, **31**(12), 146 (2012).
[17] M. C. Meyers, Dynamic Behavior of Materials, Wiley, New York, 1995.
[18] Kolsky H. Stress waves in solids. Oxford: Clarendon Press; 1953.

* Corresponding author: zhdawei@hit.edu.cn